Report Number 1

NOAA Grant NA56EC0145

Continuation and Expansion of Stereoscopic

Determination of Cloud Height and Motion

Summary of the Cloud Height and Motion Experiment (CHAMEX)

17- 28 April 1995
at
Norman, Oklahoma

James Partacz

with

T. Theodore Fujita

The University of Chicago

July 1995

Summary of CHAMEX at Norman, Oklahoma

11 days, 17-28 April 1995

Table of Contents

1. INTRODUCTION

The location of the 1995 CHAMEX was selected by Paul Menzel, NESDIS monitor and Ted Fujita, University of Chicago PI, taking into consideration the other research activities in and around Norman, Oklahoma. In an attempt to interact with Jim Purdom and Roger Wakimoto, the two weeks of April 17 and April 24 were chosen. Originally, Ted Fujita , Jim Partacz and Duane Stiegler planned to participate in the Norman experiment. Due to Fujita's eye problems caused by construction dust, the experiment was manned by Jim (south site) and Duane (north site) while keeping close contact with Fujita. (Fig 1.1)

In spite of the fact that photogrammetric cameras, including back-up cameras, were ready for operation throughout the two week period, weather in Oklahoma was unfavorable for CHAMEX for tracking predominately high clouds. Presented in this report is a summary of the cases which can be used for achieving cloud height and motion computations to be performed independently under the direction of Paul Menzel and Ted Fujita.

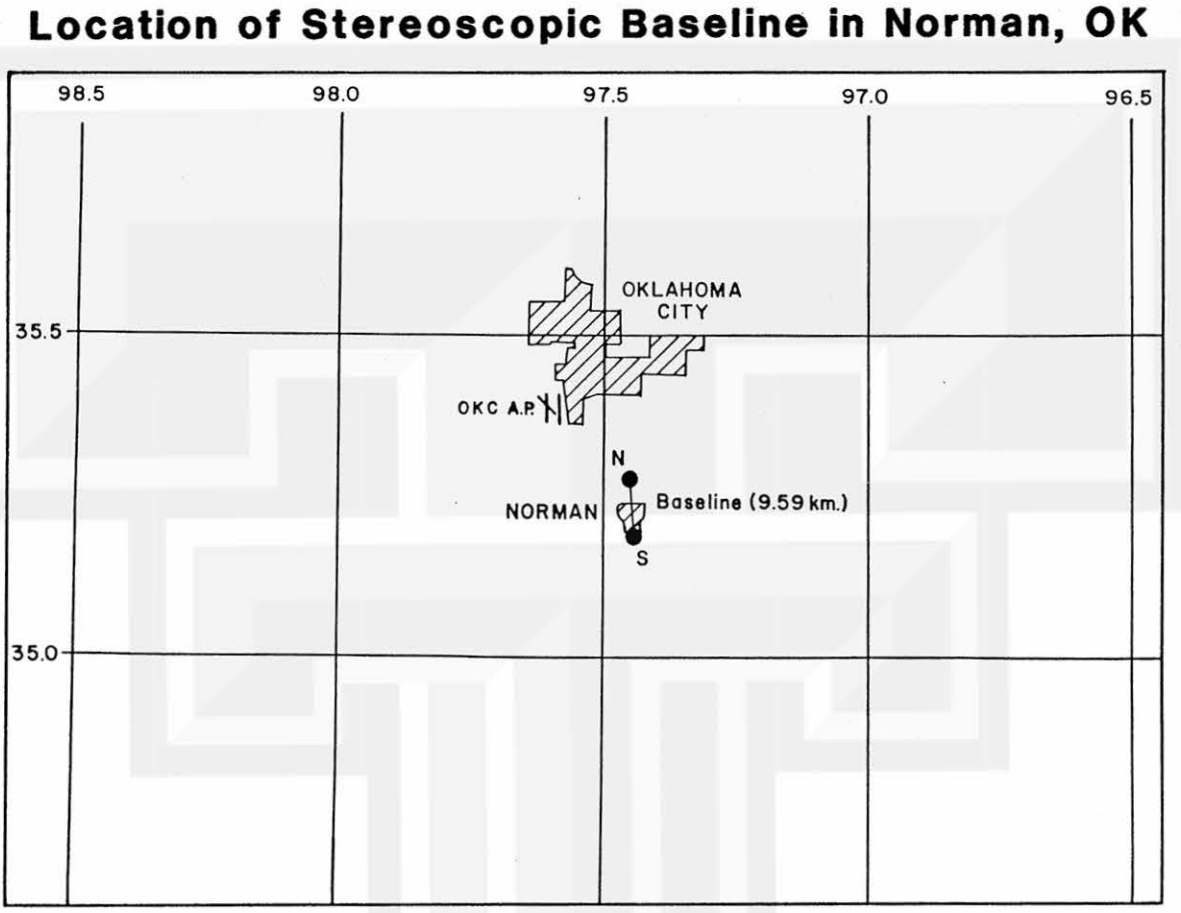

Fig. 1.1 The area of the CHAMEX 1995 , located in Oklahoma. Oklahoma City with Will Rogers Airport and Norman with the stereoscopic baseline are shown in this map.

2. SITE SELECTION FOR STEREOSCOPIC PHOTOGRAMMETRY

It was discovered in previous cloud motion studies (Chicago, Key West and Cape Hatteras), that camera location is very important in obtaining the proper images for stereoscopic photogrammetry. In addition to the safety of cameras and operators, there are two main considerations when selecting the sites.

First, the distance between the cameras, or the baseline length must be chosen so as to obtain good stereo-pair images. For high to mid-level clouds it was previously determined that the baseline should be between 8-10 km. for accurate cloud tracking.

Second, the site must be surrounded by many distinct objects that can be identified on the whole-sky image. It is also important to find these objects scattered all around the camera. This second consideration is needed to determine if the camera is pointing precisely towards the zenith, in order to obtain the accurate horizon radius for the whole-sky images. Determining the horizon radius is of the utmost importance to compute accurately, the cloud height and motion from whole-sky images.

The north site was located at the Norman-Moore Vocational School and the south site, was at the University of Oklahoma. These two places were found to be ideal in satisfying the above mentioned considerations. By mapping these sites on a 7.5-min. USGS map (Fig. 2.1) the baseline orientation was computed to be 173.7° true azimuth with the length of 9.59 km. This distance between the sites will be ideal for triangulating mostly high and some mid-level clouds.

Locations of North and South Camera Site

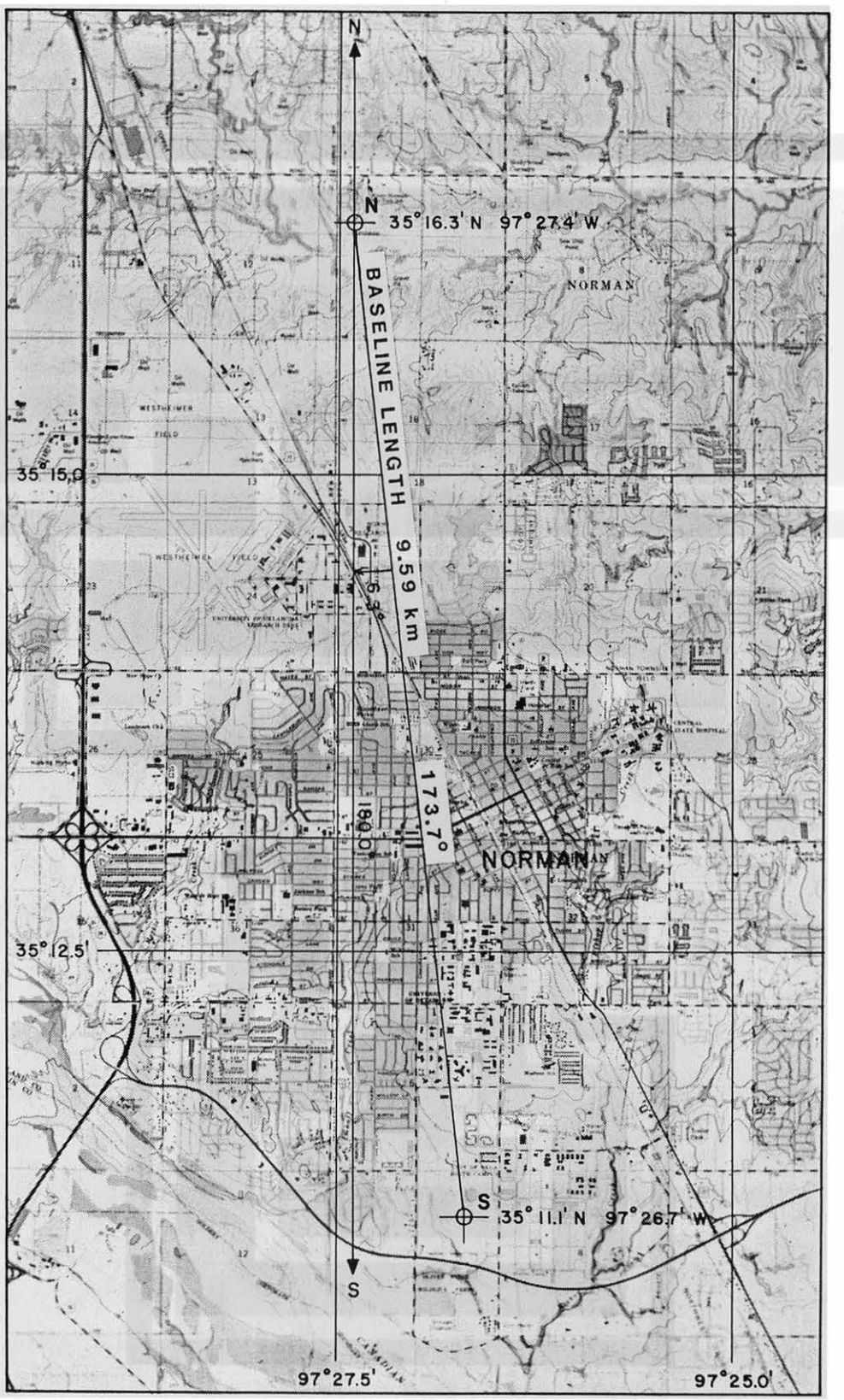

Fig. 2.1 A detailed map of the stereoscopic baseline placed across Norman, Oklahoma. The North Site(N) is located at the Norman-Moore Vocational School and the South Site(S) on University of Oklahoma property. The baseline orientation is 173.7° true azimuth with length of 9.59 km. This separation was selected to triangulate high clouds to be depicted by the moisture channel of GOES 8.

3. METHOD OF DETERMINING THE HORIZON RADII OF WHOLE-SKY PICTURES

It is important to determine the precise horizon radius of each whole-sky picture. Unfortunately the radius cannot simply be measured on the picture because the maximum zenith angle in the whole-sky imagery is 1° to 2° less than 90°. This is mostly due to the haze/smog conditions that act to obscure the outer edge on the whole-sky picture. The steps to determine the horizon radius are to print black and white pictures of whole-sky images and to identify a large number of objects with various azimuths at each site. Both sites in Norman had plenty of objects, with 32 at the north site and 21 at the south.(Fig. 3.1-3.2)

Four panoramic pictures were taken from the exact position of the whole-sky lens, using a Widelux camera with a 130° field of view. These pictures were then put together to form a composite 360° panoramic picture at each site. Knowing the exact location of each site and measuring the length of the 360° panoramic picture, the azimuth and elevation angles can be computed and overlaid on the panoramic picture(Fig. 3.3).

The identical objects seen in the whole-sky image are now identified on the panoramic picture. Azimuth and elevation angles are then measured for each object at both sites from the panorama and are shown in Tables 3.1 and 3.2. The location of these objects are also measured from the whole-sky picture in the 0.05" units. With the zenith at the origin of the rectangular coordinates, a and b are measured, where a denotes the abscissa, positive toward the west and b, the ordinate, positive in the direction of the baseline, toward the north. For each object a zenith angle(ζ) is found by subtracting the elevation angle found on the panorama from 90°. Using these values the horizon radius(R) for each object were computed. (Fig. 3.4)

Under perfect situation, the horizon radii from different objects should be identical. However, due to the inevitable error in determining elevation angles, the computed radii may vary by a small amount. Even if this variation is small the error should be checked if the difference is due to improper alignment of the optical axis of the whole-sky lens pointing toward the zenith. This was checked by plotting the horizon radii against the

azimuth of each object, shown in Figs. 3.5-3.6. These charts show the radii for both sites varied independent of the azimuth and therefore indicating that the whole-sky lens was correctly pointing toward the zenith.

To show just how small the differences between radii for each site were, histograms were made with the computed horizon radii of the 32 objects at the north and 21 objects at the south sites. (Fig. 3.7) It is seen that the north image is 1.3% larger than the south image. This is due to the difference in the size of each picture when it was printed, which is normal and not an error. More importantly however, it is shown that the radii at each site fall closely to the average. This means that the average horizon radius obtained for both the north and south sites can be used in the computation of cloud height and motion from whole-sky stereo-pair pictures.

NORTH SITE

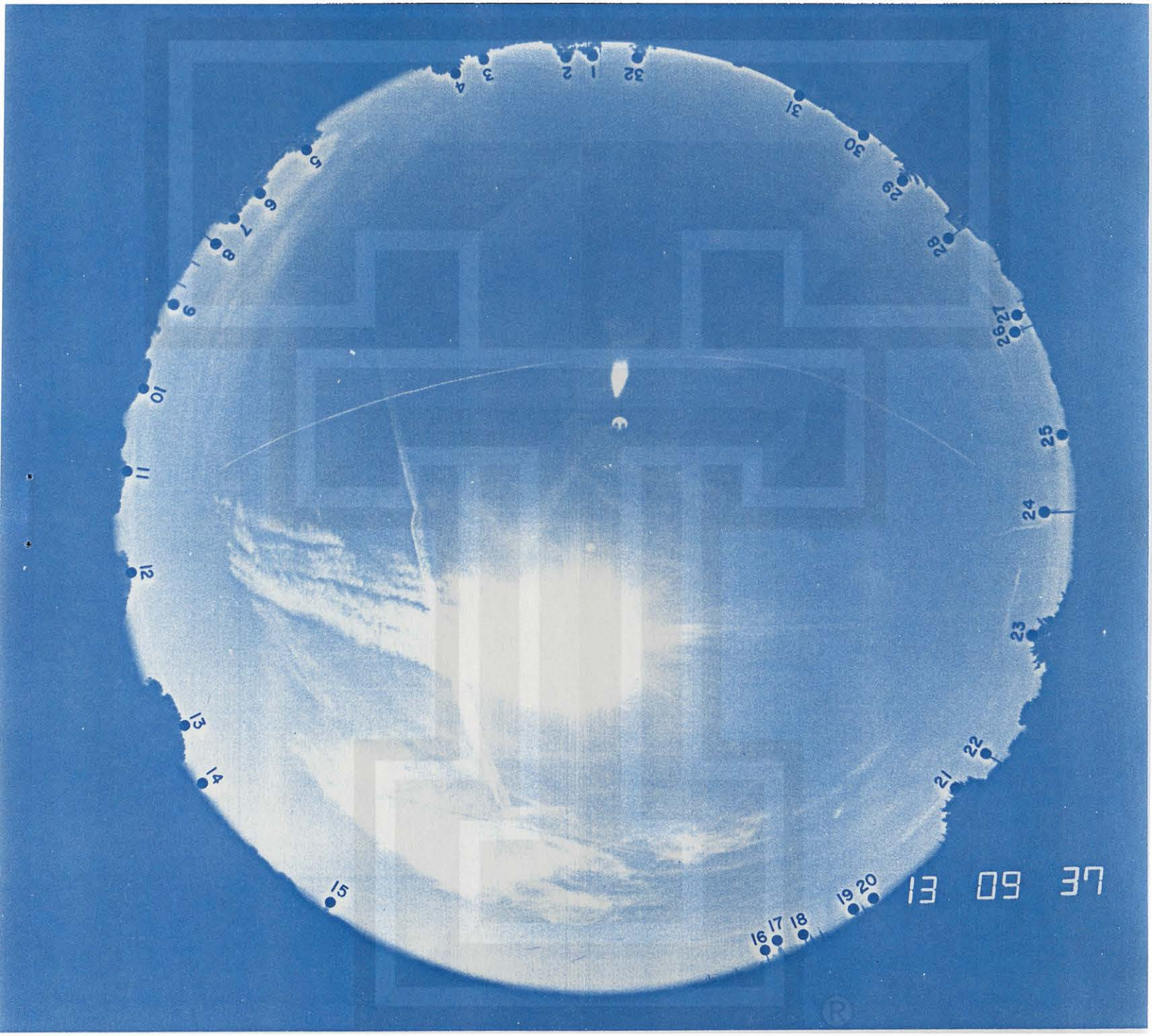

Fig. 3.1 Whole-sky image from the North Site showing the 32 identified objects. Each of these objects was located on the panoramic pictures taken at the North Site.

SOUTH SITE

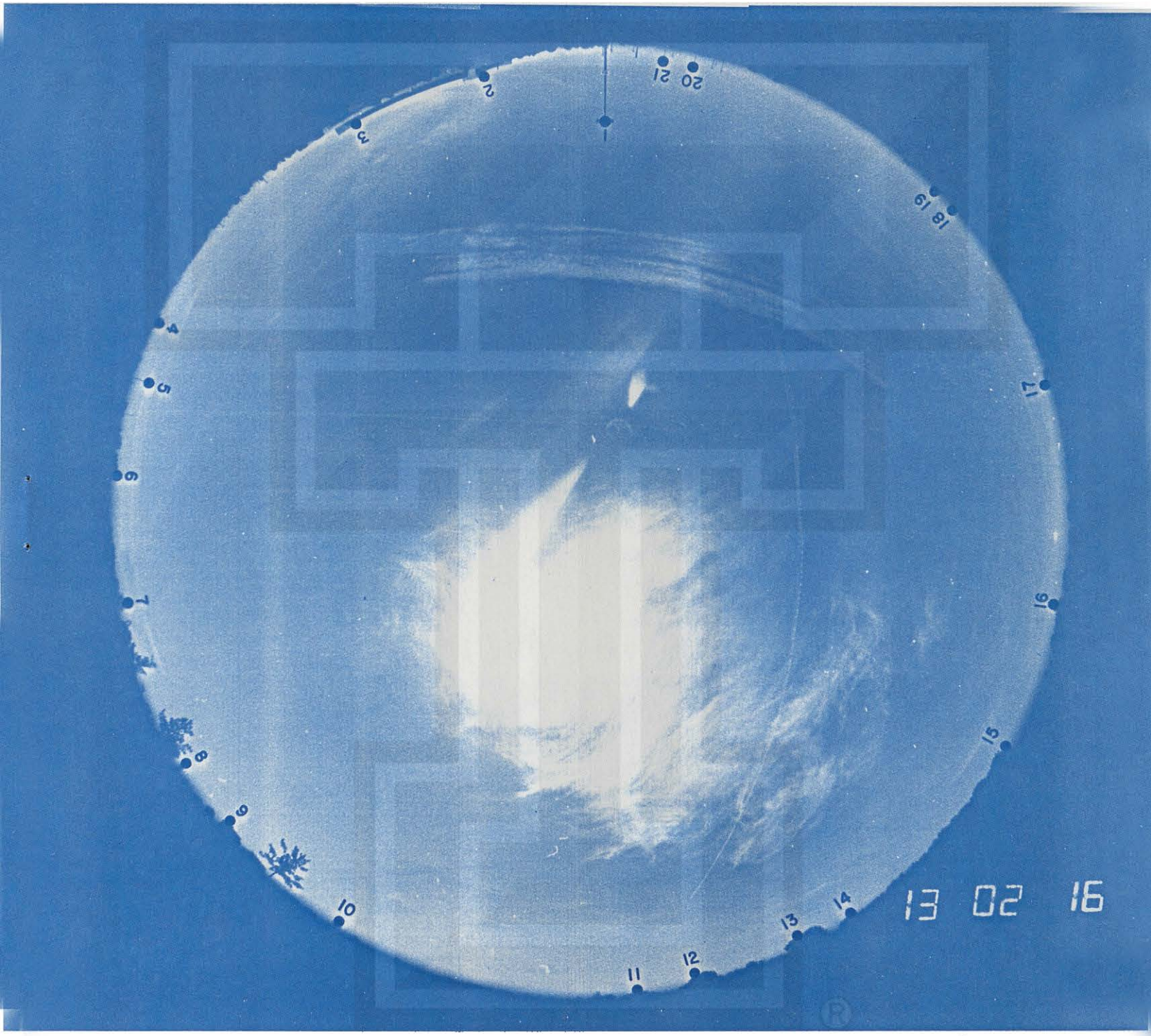

Fig. 3.2 Whole-sky image from the South Site showing the 21 identified objects. Each of these objects was located on the panoramic pictures taken at the South Site.

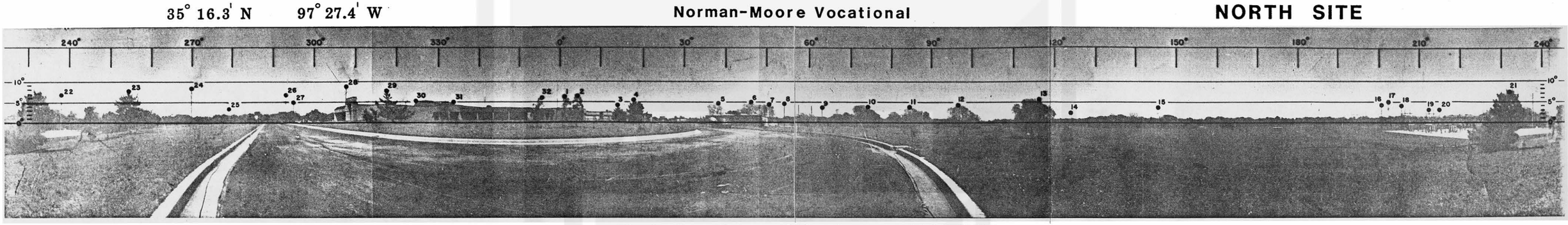

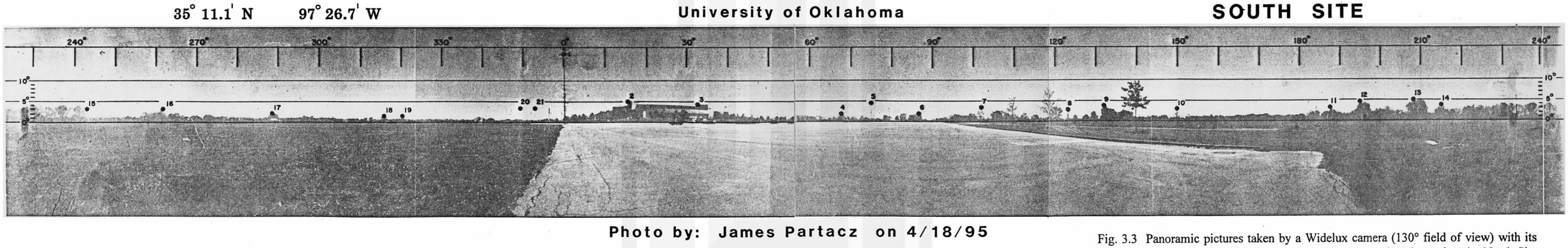

Fig. 3.3 Panoramic pictures taken by a Widelux camera (130° field of view) with its lens placed at the exact position of the whole-sky camera lens located at the North Site (upper) and South Site (lower). The top scale denotes azimuth angles for the panorama. On both sides of the panorama are elevation angles. Distant objects numbered and identified from the whole-sky images are also shown.

Horizon Radii of Whole-sky Imagery Computed From Panoramic Picture

NORTH SITE

	Panaramic Pjcture				Whole-sky Picture			
	β	ε	ζ		a	b	c	R
I.D.	Azimuth (deg)	Elevation (deg)	Zenith (deg)	Description	(x 0.05")	(x 0.05")	$\sqrt{a^2+b^2}$ (x 0.05")	Horizon Radius (x 0.05")
1	1.0	6.1	83.9	Tree	-8.0	66.9	67.4	72.28
2	4.2	6.2	83.8	Tree	-11.8	66.4	67.4	72.43
3	14.1	4.0	86.0	Tree	-24.0	64.9	69.2	72.41
4	17.8	5.4	84.6	Tree	-27.9	62.3	68.3	72.62
5	38.2	4.6	85.4	Tree	-48.5	49.0	68.9	72.66
6	46.2	5.0	85.0	Tree	-54.7	41.8	68.8	72.89
7	50.6	4.3	85.7	Tree	-57.9	37.5	69.0	72.44
8	54.2	4.6	85.4	Utility pole	-60.0	33.8	68.9	72.57
9	63.0	3.6	86.4	Utility pole	-65.4	24.2	69.7	72.64
10	74.0	3.7	86.3	Tree	-68.6	11.4	69.5	72.52
11	84.4	3.8	86.2	Tree	-69.7	-0.9	69.7	72.78
12	96.6	4.1	85.9	Tree	-67.6	-15.6	69.4	72.69
13	116.3	5.5	84.5	Tree	-57.4	-37.1	68.3	72.79
14	124.1	2.3	87.7	High tension tower	-54.0	-45.5	70.6	72.47
15	145.5	3.5	86.5	High tension tower	-33.5	-61.1	69.7	72.50
16	200.5	4.0	86.0	Electric pole	30.9	-61.9	69.2	72.40
17	202.3	5.0	85.0	High tension tower	32.5	-60.2	68.4	72.44
18	205.6	3.9	86.1	Electric pole	36.3	-59.0	69.3	72.41
19	212.4	3.0	87.0	Electric pole	43.4	-54.8	69.9	72.31
20	215.1	3.0	87.0	Electric pole	46.0	-52.7	70.0	72.36
21	232.0	7.2	82.8	Tree	56.7	-35.2	66.7	72.54
22	237.7	6.7	83.3	Electric pole	60.4	-29.6	67.3	72.67
23	254.3	7.6	82.4	Tree	65.5	-11.4	66.5	72.62
24	269.8	8.2	81.8	Electric pole	65.5	6.9	65.9	72.46
25	279.1	3.2	86.8	Electric pole	67.2	18.3	69.6	72.21
26	293.1	6.7	83.3	Light pole	58.2	32.8	66.8	72.18
27	294.9	4.9	85.1	Light pole	58.5	35.4	68.4	72.31
28	307.8	8.8	81.2	Electric pole	47.2	45.6	65.6	72.74
29	317.5	7.5	82.5	Tree	39.5	53.4	66.4	72.46
30	324.6	5.1	84.9	Building	33.1	59.5	68.1	72.18
31	333.7	4.9	85.1	Building	23.0	64.3	68.3	72.22
32	355.7	5.9	84.1	Tree	-1.4	67.6	67.6	72.36
							Average	**72.49**

Table 3.1 The characteristics of 32 objects identified in whole-sky pictures taken at the North Site. The azimuth and elevation angles were computed from the panoramic pictures, a and b were measured from the whole-sky picture, b-ordinate being positive in the direction of the baseline and a-abscissa positive towards the west .

Because the maximum zenith angle seen in the whole-sky pictures is less than 90°, the radius of the invisible horizon circle was computed from the elevation angle of each object. Due to the inevitable error in determining elevation angles, computed radii vary with azimuth.

Horizon Radii of Whole-sky Imagery Computed From Panoramic Picture

SOUTH SITE

	Panaramic Picture				Whole-sky Picture			
	α	ε	ζ		a	b	c	R
I.D.	Azimuth (deg)	Elevation (deg)	Zenith (deg)	Description	(x 0.05")	(x 0.05")	$\sqrt{a^2+b^2}$ (x 0.05")	Horizon Radius (x 0.05")
1	0.1	16.5	73.5	Light pole	-6.8	58.6	59.0	72.24
2	15.5	4.9	85.1	Building	-25.1	63	67.8	71.72
3	32.5	4.3	85.7	Building	-42.8	53.1	68.2	71.62
4	67.4	1.9	88.1	Dome	-67.1	19.9	70.0	71.50
5	74.6	4.6	85.4	Light pole	-67.1	11.3	68.0	71.71
6	86.4	2.1	87.9	Trees	-70.0	-2.6	70.0	71.72
7	101.8	3.5	86.5	Trees	65.6	-20.7	68.8	71.57
8	123.0	3.2	86.8	Water tower	-54.0	-42.9	69.0	71.51
9	131.8	3.7	86.3	Trees	-46.5	-50.4	68.6	71.51
10	149.8	3.1	86.9	Trees	-28.8	-62.9	69.2	71.65
11	187.4	3.3	86.7	Trees	15.8	-67	68.8	71.46
12	194.8	4.6	85.4	Trees	23.9	-63.5	67.8	71.50
13	208.3	5.1	84.9	Trees	38.0	-55.8	67.5	71.57
14	215.0	3.8	86.2	Trees	45.2	-51.5	68.5	71.54
15	243.0	3.1	86.9	Trees	64.8	-24.1	69.1	71.60
16	261.7	3.2	86.8	Trees	68.8	-2.7	68.9	71.39
17	288.4	2.1	87.9	Trees	63.2	29.2	69.6	71.28
18	315.7	1.5	88.5	Trees	43.1	55.5	70.3	71.46
19	320.3	1.5	88.5	Trees	38.8	58.6	70.3	71.47
20	349.2	3.4	86.6	Light pole	4.9	68.7	68.9	71.58
21	353.1	3.5	86.5	Light pole	0.6	68.9	68.9	71.69
							Average	**71.59**

Table 3.2 The characteristics of 21 objects identified in whole-sky pictures taken at the South Site. The azimuth and elevation angles were computed from the panoramic pictures, a and b were measured from the whole-sky picture, b-ordinate being positive in the direction of the baseline and a-abscissa positive towards the west .

Because the maximum zenith angle seen in the whole-sky pictures is less than 90°, the radius of the invisible horizon circle was computed from the elevation angle of each object. Due to the inevitable error in determining elevation angles, computed radii vary with azimuth.

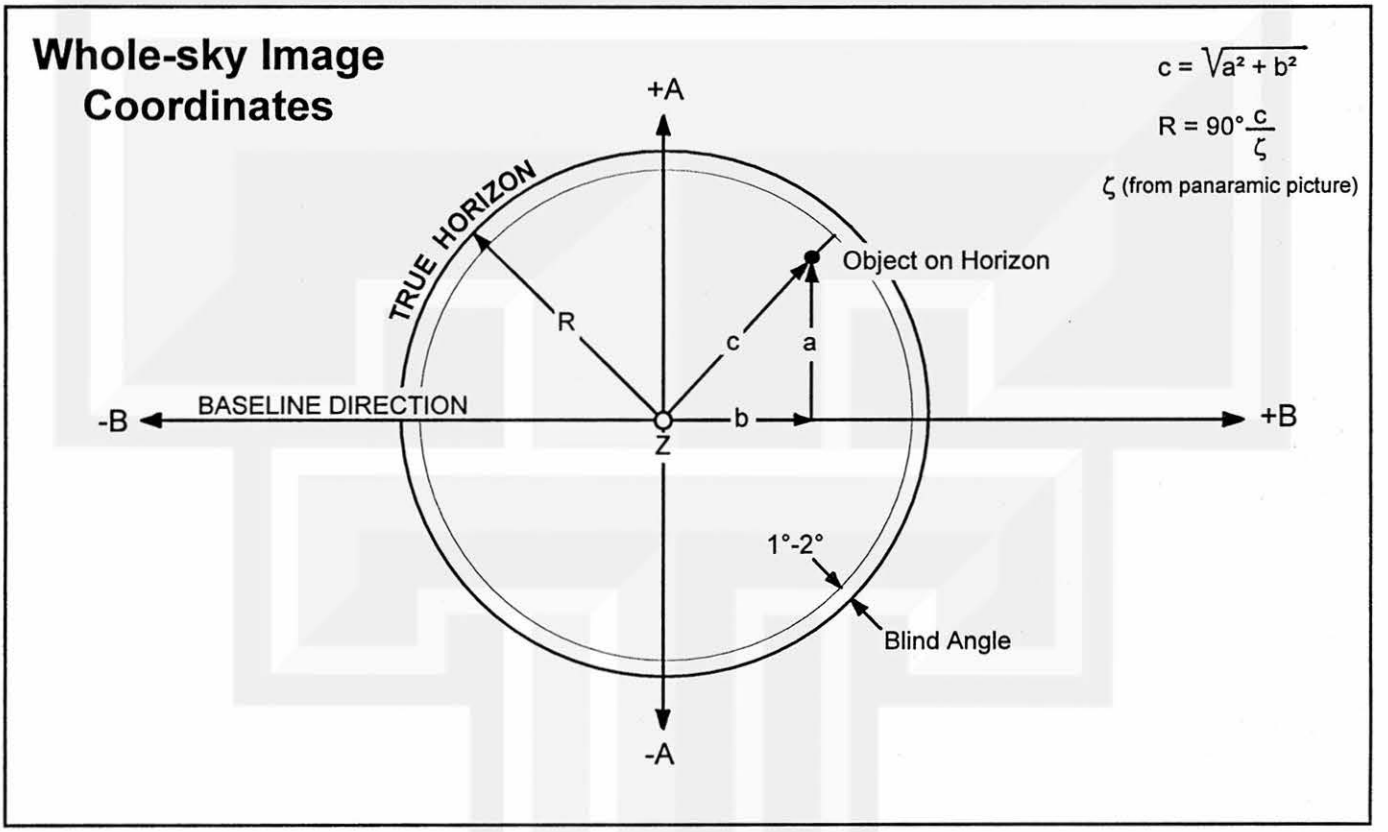

Fig. 3.4 After computing the zenith angle (ζ) from the panoramic picture, then measuring the whole-sky coordinates a and b(0.05"), it is possible to compute a horizon radius (R) for each object.

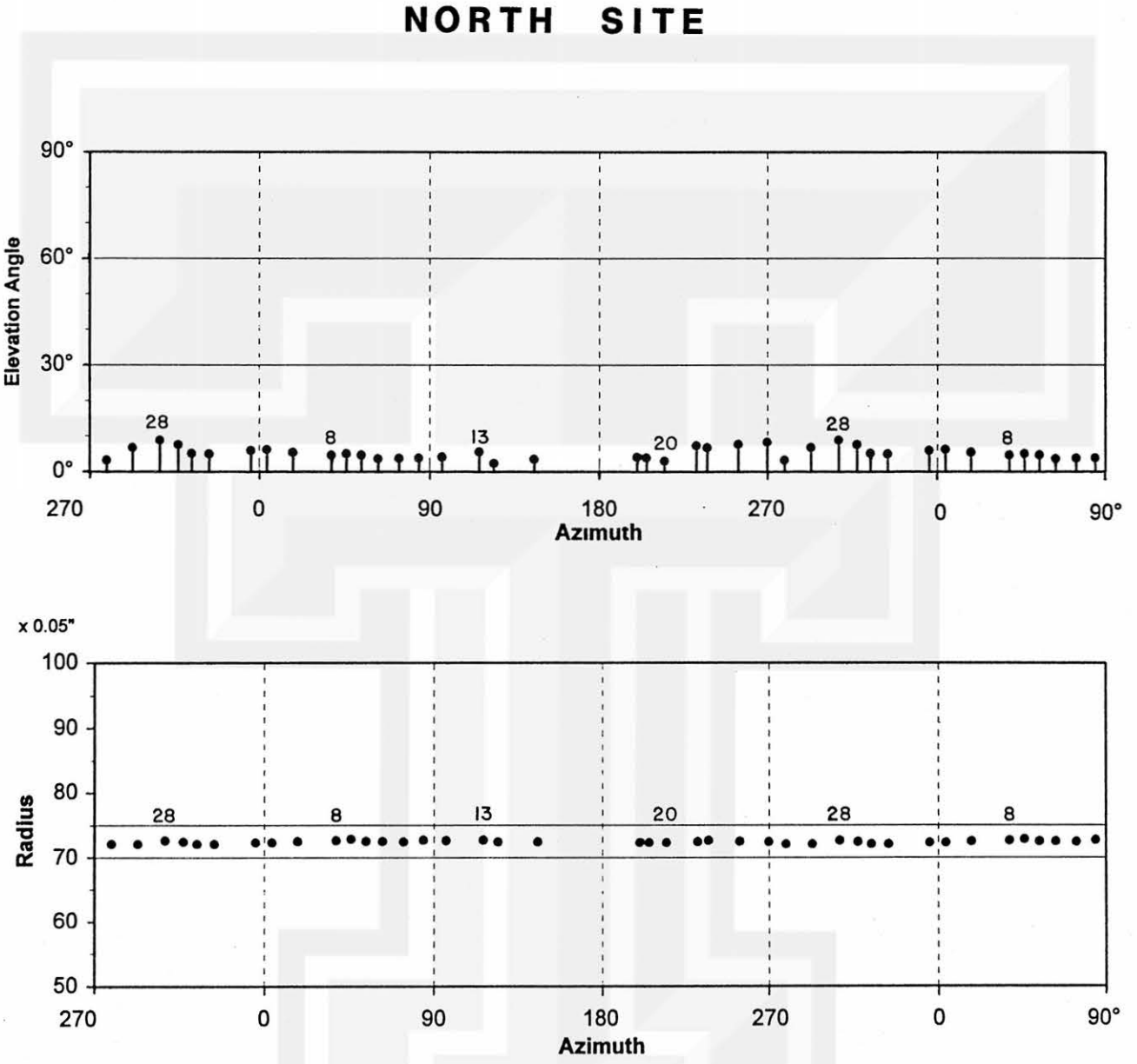

Fig. 3.5 The upper chart shows 32 objects, as painted circles placed at their azimuth and elevation angle coordinates. The horizon radii computed as a function of the azimuths of the objects, as shown in the lower chart. Note that horizon radii did not vary with azimuth, indicating the optical axis of the whole-sky lens pointed toward the zenith.

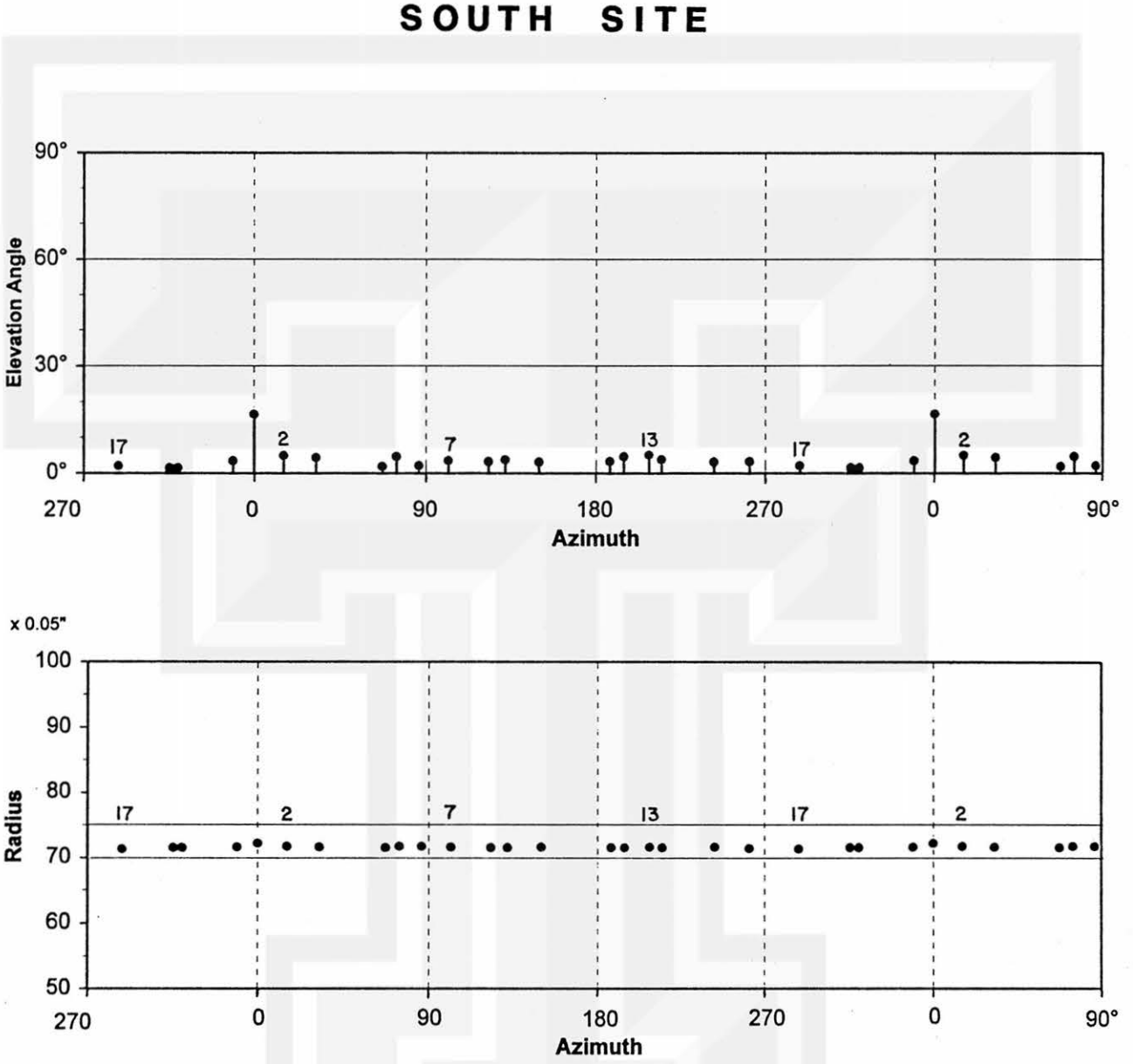

Fig. 3.6 The upper chart shows 21 objects, as painted circles placed at their azimuth and elevation angle coordinates. The horizon radii computed as a function of the azimuths of the objects, are shown in the lower chart. Note that horizon radii did not vary with azimuth, indicating the optical axis of the whole-sky lens pointed toward the zenith.

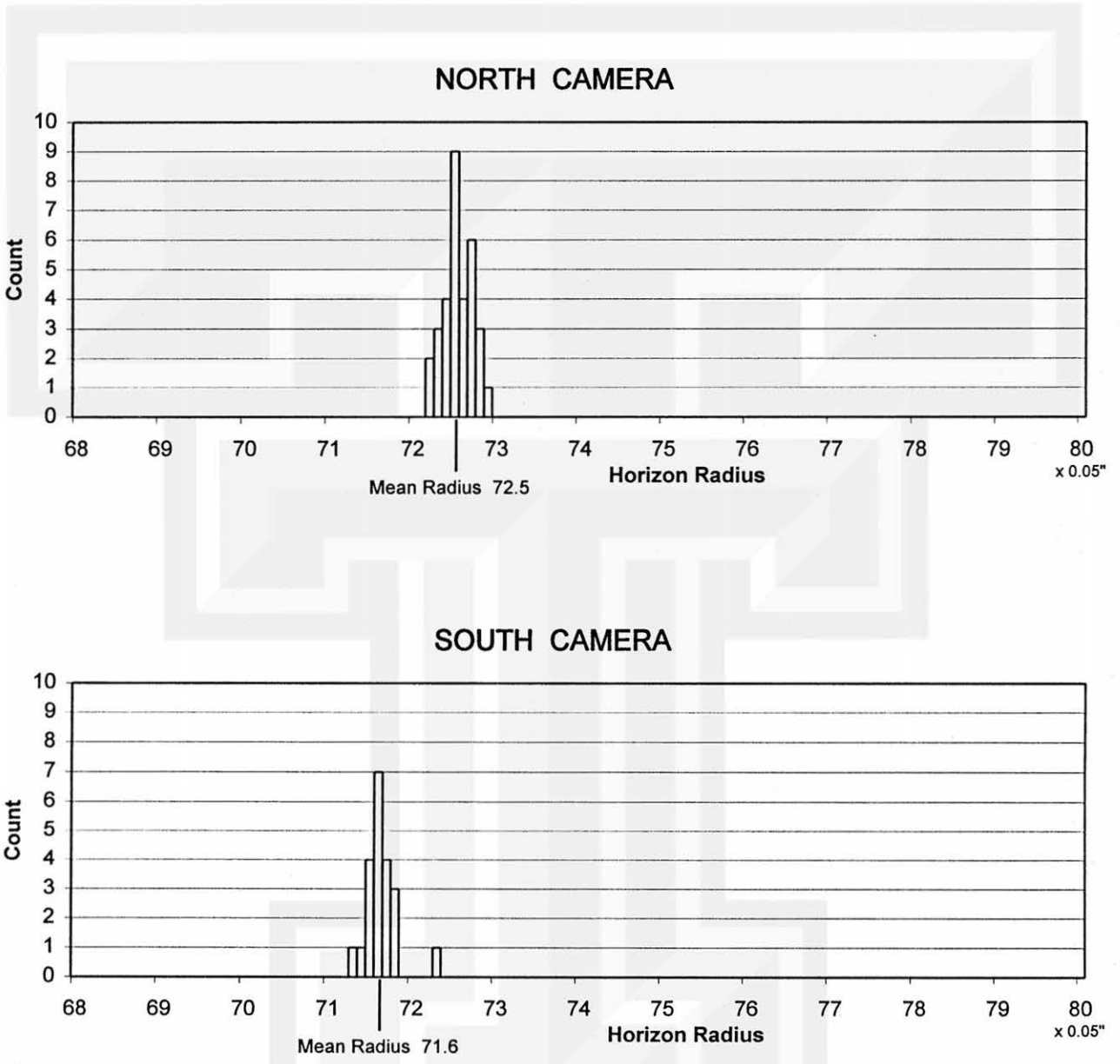

Fig. 3.7 Histograms of the horizon radii computed from the 32 objects identified in the North image(upper) and from the 21 objects in the South image(lower) reveal that the size of the North image happened to be 1.3% larger than that of the South image. After determining the mean radii of North and South images stereo-pairs are ready to use for cloud height and motion computations.

4. CHRONOLOGICAL SUMMARY OF THE FIELD EXPERIMENT

A major reason that Norman, Oklahoma was chosen as the site of CHAMEX 1995 was the ability to get rapid-scan satellite imagery which was expected to be used for the VORTEX project. The rapid-scan time was set between 1315-1600 CST each day. The scan time was decided before leaving Chicago and it was agreed that CHAMEX follows the same schedule. Although the rapid-scan time could not be altered, the whole-sky cameras could be started with as little as one-half hour advanced notice.

As mentioned in the introduction, the weather did not produce many high clouds, especially during rapid-scan time. It was decided that on the day when high clouds are expected prior to 1315 CST, the whole-sky cameras are turned on earlier, hoping that the high clouds will continue into the rapid-scan period.

On most days the appearance of high clouds was non-existent, either because of low overcast or clear skies. However, stereo whole-sky pictures were taken on five days, with the best day being 27 April with three hours of whole-sky pictures and rapid-scan data. Although there was only one day with complete rapid-scan coverage, the other days could be analyzed as well and compared to regular satellite imagery.

A complete 11-day log with potential research cases numbered and underlined is shown in Table 4.1. A more detailed chronological chart showing the five days that stereo whole-sky pictures were taken along with a rating for cloud conditions is shown in Fig. 4.1.

Potential Research Cases of Cloud-motion Computations

Norman, OK Network April 17-28, 1995

(Rapid-scan Period 1315-1600 CST)

Potential Cases

4/17/95 **Photographic Periods: (None)** Overcast with rain and thunder showers all day.

4/18/95 **Photographic Periods: (None)** Clear skies all day.

1. 4/19/95 **Photographic Periods: (1131-1349 CST)** 2 minute intervals. Multi-layer clouds before scheduled start time with increasing low clouds, making it difficult to track any high clouds.

4/20/95 **Photographic Periods: (None)** Mostly clear with scattered low clouds all day.

4/21/95 **Photographic Periods: (None)** Clear skies all day.

4/22/95 **Photographic Periods (None)** Rain and thunderstorms all day.

4/23/95 **Photographic Periods (None)** Overcast with some breaks in overcast all day.

2. 4/24/95 **Photographic Periods (1315-1430 CST)** 2 minute intervals. Breaks in low clouds with upper level clouds visible occasionally.

3. 4/25/95 **Photographic Periods (1215-1600 CST)** 2 minute intervals. Good, trackable multi-level cirrus and alto-cumulus before 1315 CST, but mostly clear skies with more distant cirrus bands during rapid-scan.

4. 4/26/95 **Photographic Periods (1215-1615 CST)** 2 minute intervals. Mostly low cloud overcast all day, with some high clouds visible.

5. 4/27/95 **Photographic Periods (1315-1615 CST)** 2 minute intervals. Very good trackable cirrus with some mid-level clouds and contrails.

4/28/95 **Photographic Periods (None)** Overcast skies all day.

Table 4.1 A list of each day available to take whole-sky pictures. The five days of actual stereoscopic pictures are underlined and identified **1.-5.** A more detailed description can be found on pages 19-33.

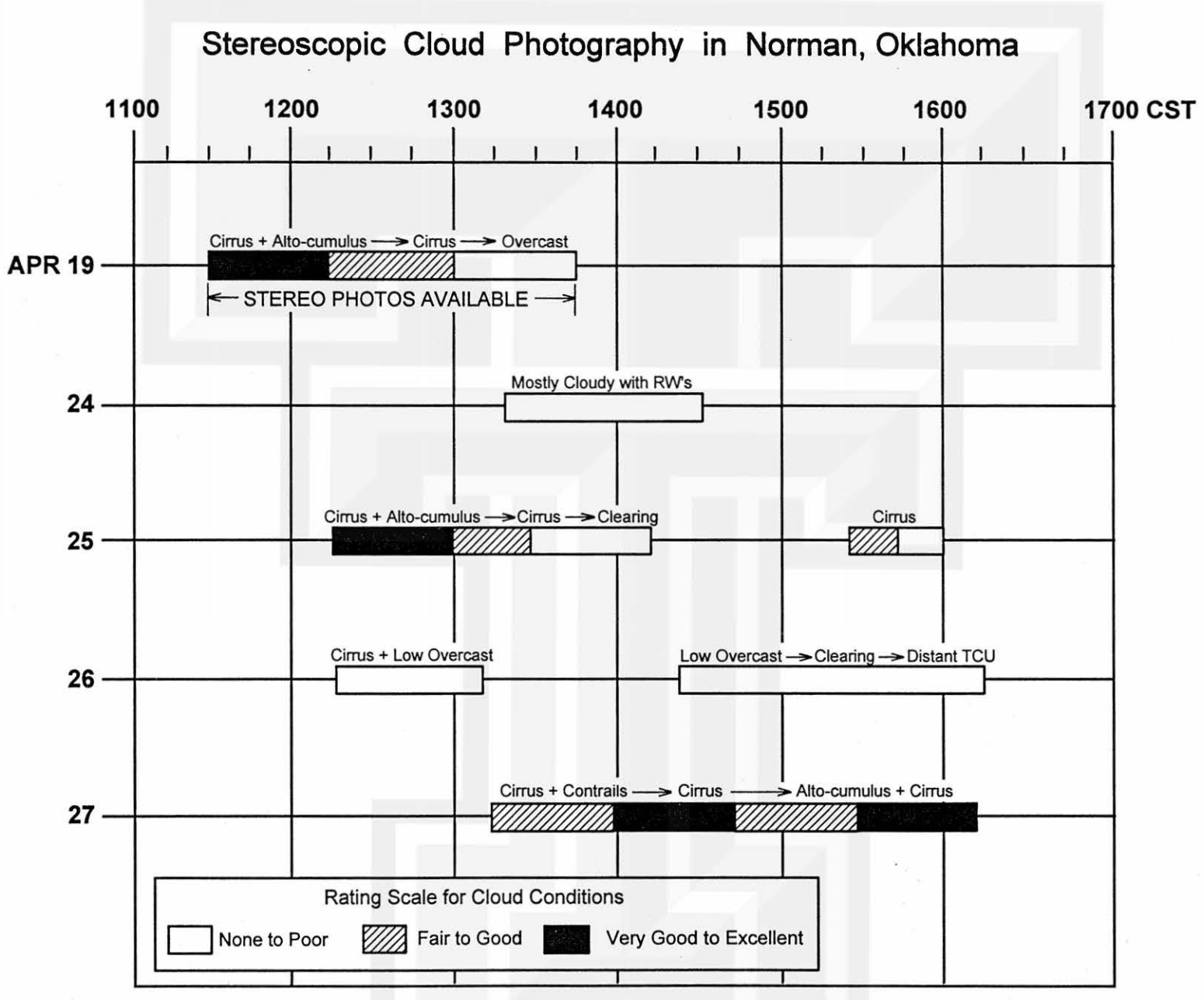

Fig. 4.1 Chronological chart showing the five days where stereoscopic cloud photography was undertaken and are the potential cases for determining cloud height and motion. The rating scale takes into account the type of cloud and the ability to track it.

5. POTENTIAL RESEARCH CASES

Each day that the whole-sky cameras were in operation is treated as a potential research case. Shown in the previous chapter, Table 4.1 and Fig. 4.1, the whole-sky cameras were operated on five days when high and middle clouds were observed.

The following 15 pages (pgs. 20-34) present each case, numbered 1-5, with a more detailed description of the type of high and middle clouds that were observed, as well as the best time of trackable clouds for use in stereoscopic analysis. Following each description are one pair of stereoscopic pictures that best show the type of clouds that were observed during the period of whole-sky camera operation. The length of operation differed for each case, due to the type of cloud conditions, but the interval between whole-sky pictures was always 2-minutes. Depending on what case and cloud conditions that occurred, there are sometimes as many as 150 stereoscopic picture pairs to choose from.

Therefore, the stereo pairs shown in Figs. 5.1-5.10 are only a sample of what was collected for each case, there are many more stereoscopic pictures that could be used in determining cloud height and motion.

Case 1: Cirrus and Alto-cumulus

April 19, 1995 1131-1349 CST Cirrus and alto-cumulus were in abundance early in the period with some scattered cumulus invading the area by 1220 CST. Conditions changed rapidly after 1300 CST however, as strong winds brought in low clouds from the southwest. The cirrus had moved too far on the horizon and it became overcast by 1320 CST and remained until the operation was halted for the day. The best period for tracking high clouds was between 1131-1300 CST which is before the rapid-scan satellite pictures were available. (Figs. 5.1-5.2)

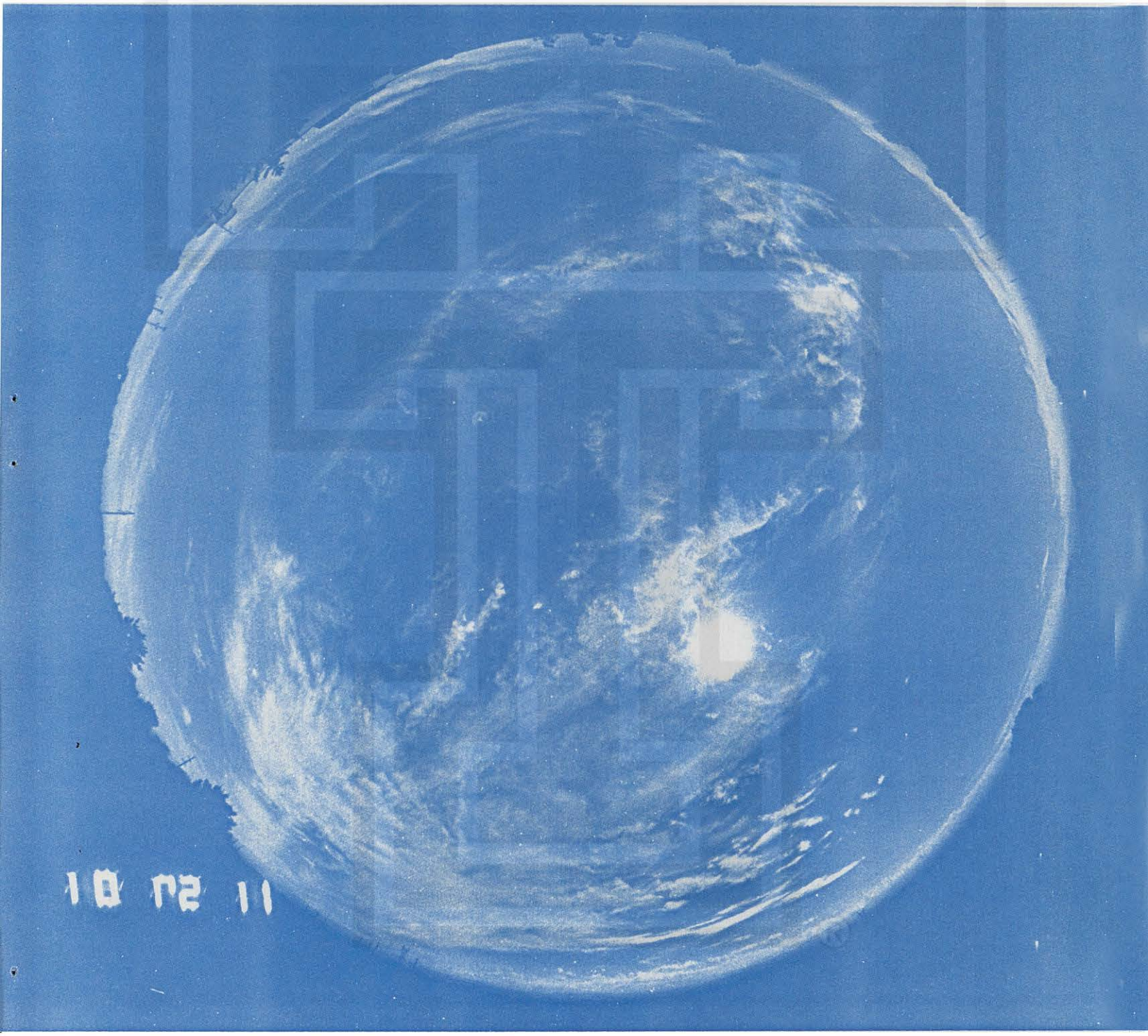

Fig. 5.1

1157 C 19 Apr 95 South

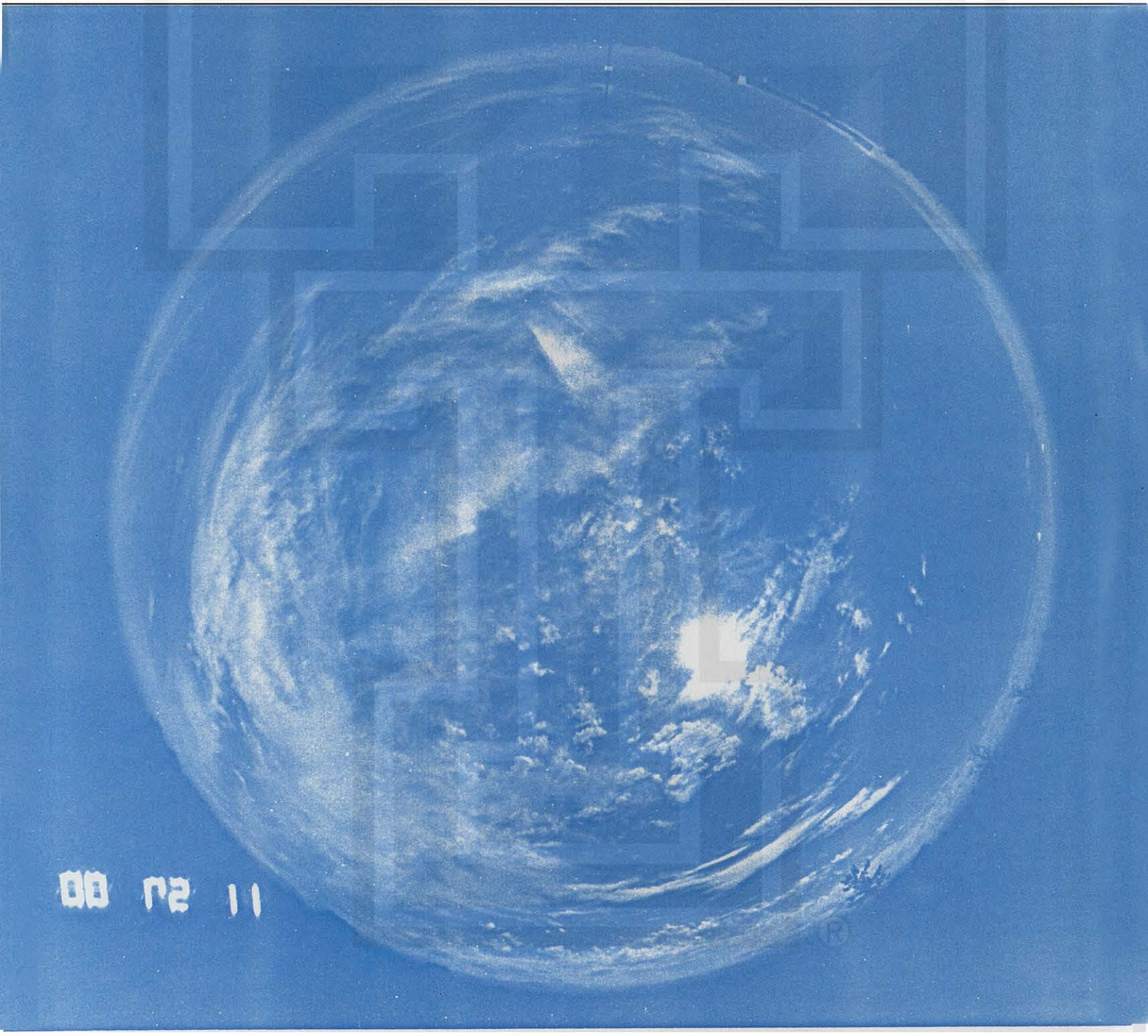

Fig. 5.2

Case 2: Cirrus Briefly Visible Through Overcast

April 24, 1995 1315-1430 CST A more stagnant situation with many low clouds obscuring the cirrus that barely could be seen through breaks in the overcast. Some rain showers at the South Site prevented stereo pictures until 1342 CST. At this time however, the skies became totally overcast and that made it impossible to continue the operation. Because of the rain showers and many low clouds interfering with the visibility of cirrus, this would be an extremely limited day for cloud tracking. (Figs. 5.3-5.4)

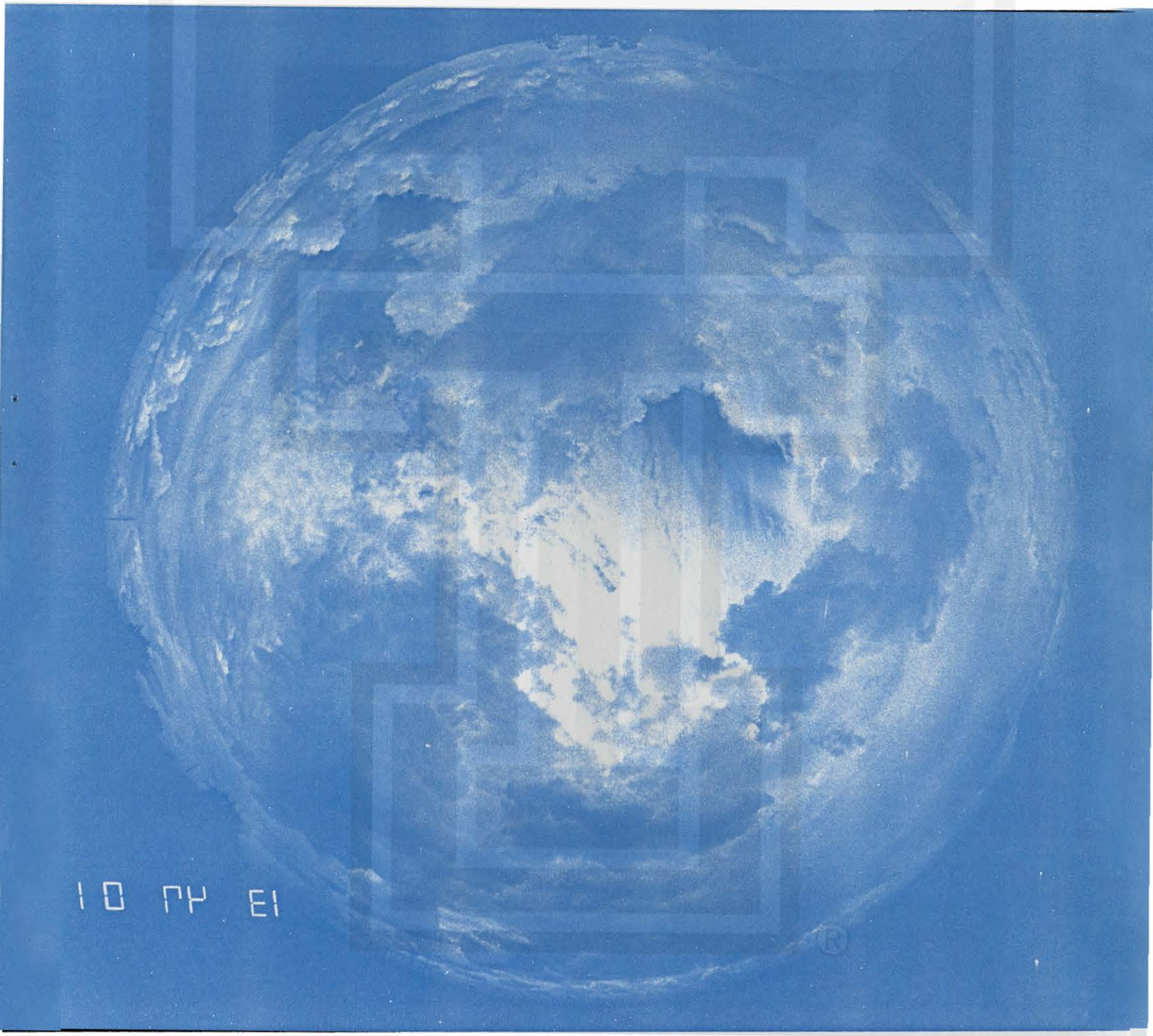

Fig. 5.3

1347 C 24 Apr 95 South

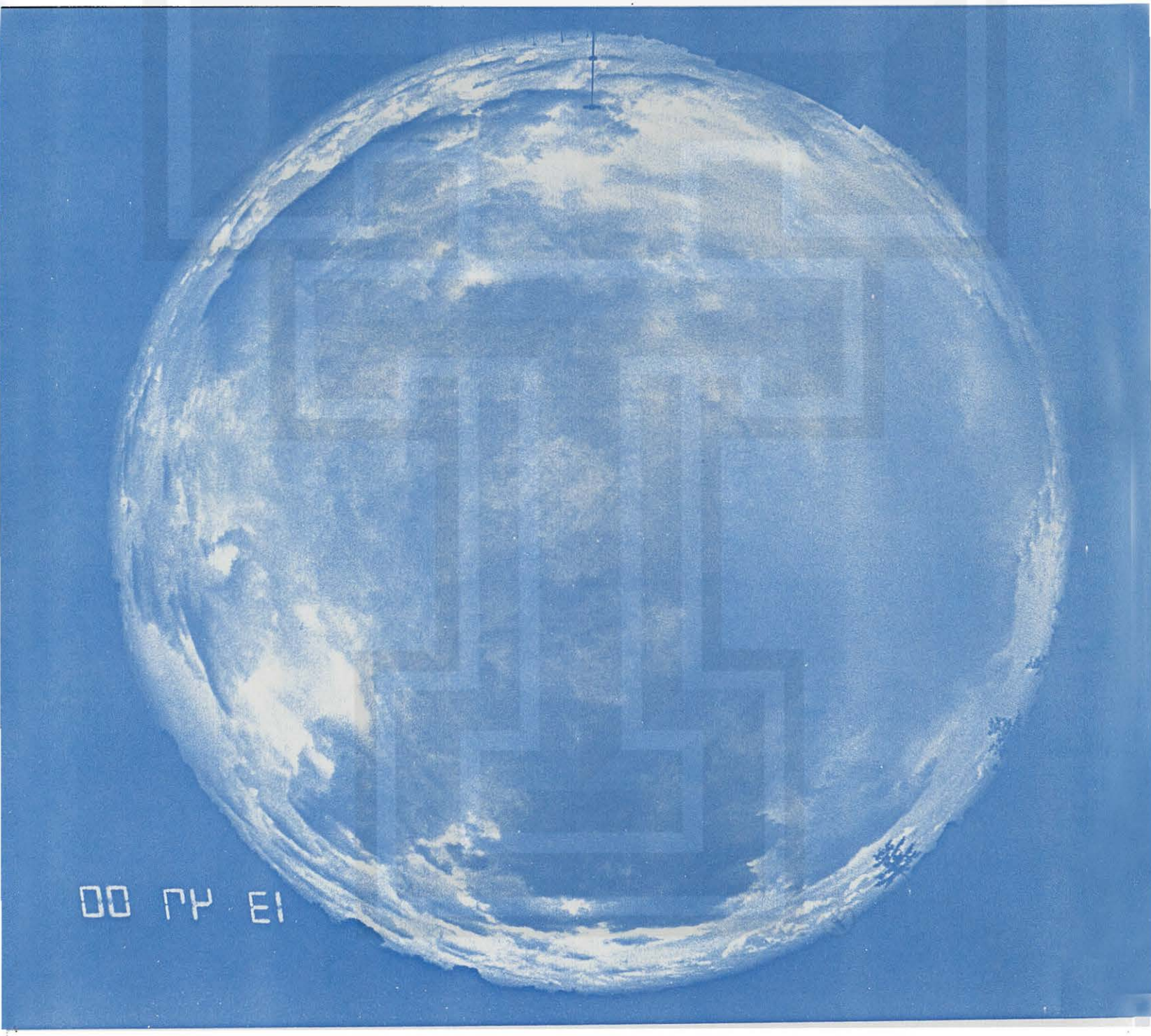

Fig. 5.4

Case 3: Cirrus and Alto-cumulus

April 25, 1995 1215-1600 CST Conditions were very good with trackable cirrus in all directions and small alto-cumulus to the east from 1215-1310 CST. Afterwards skies became increasingly clear with the cirrus moving too far on the horizon to track. Skies remained mostly clear from 1311-1430 CST until a deck of cirrus became barely trackable on the north horizon. These conditions continued until the end of operation at 1600 CST. Conditions were ideal before the rapid-scan satellite pictures were taken (1315 CST), however some tracking could be performed between 1315-1330 and again at 1500-1530 CST although the cirrus was very minor and far on the horizon. (Figs. 5.5-5.6)

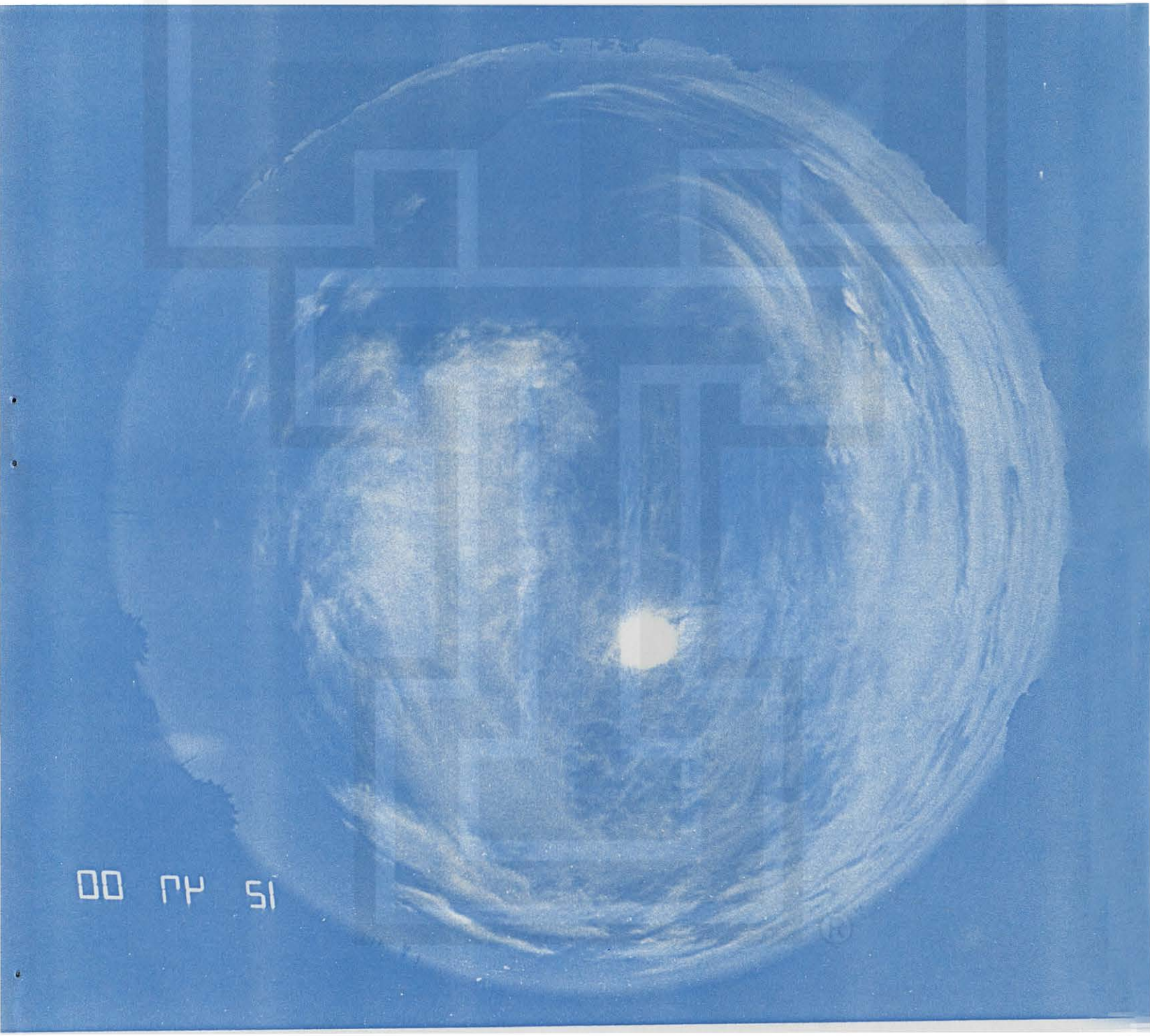

Fig. 5.5

1247 C 25 Apr 95 South

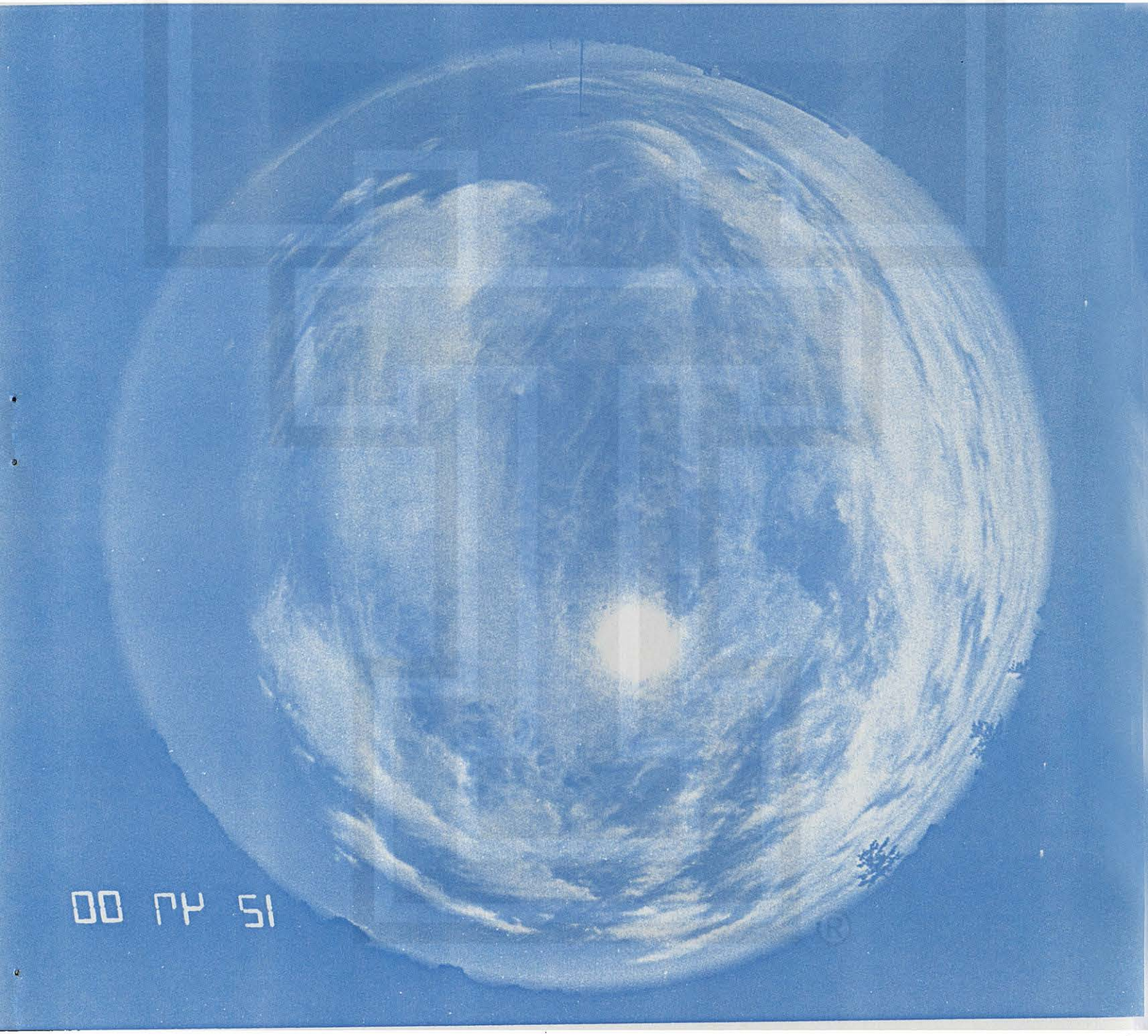

Fig. 5.6

Case 4: Cirrus and Distant Squall-line

April 26, 1995 1215-1615 CST Some alto-stratus might have been trackable early on, but they were obscured by too many fast moving low clouds. These conditions continued until 1530 CST when a fast moving cold front came overhead and cleared skies rapidly. By 1545 CST skies began clearing which revealed the back line of towering cumulus cloud tops to the east-southeast, but no visible high or mid-level clouds to track. The only possible tracking on this day would be the cumulus line after the front passed and skies cleared, but this would be very limited. (Figs. 5.7-5.8)

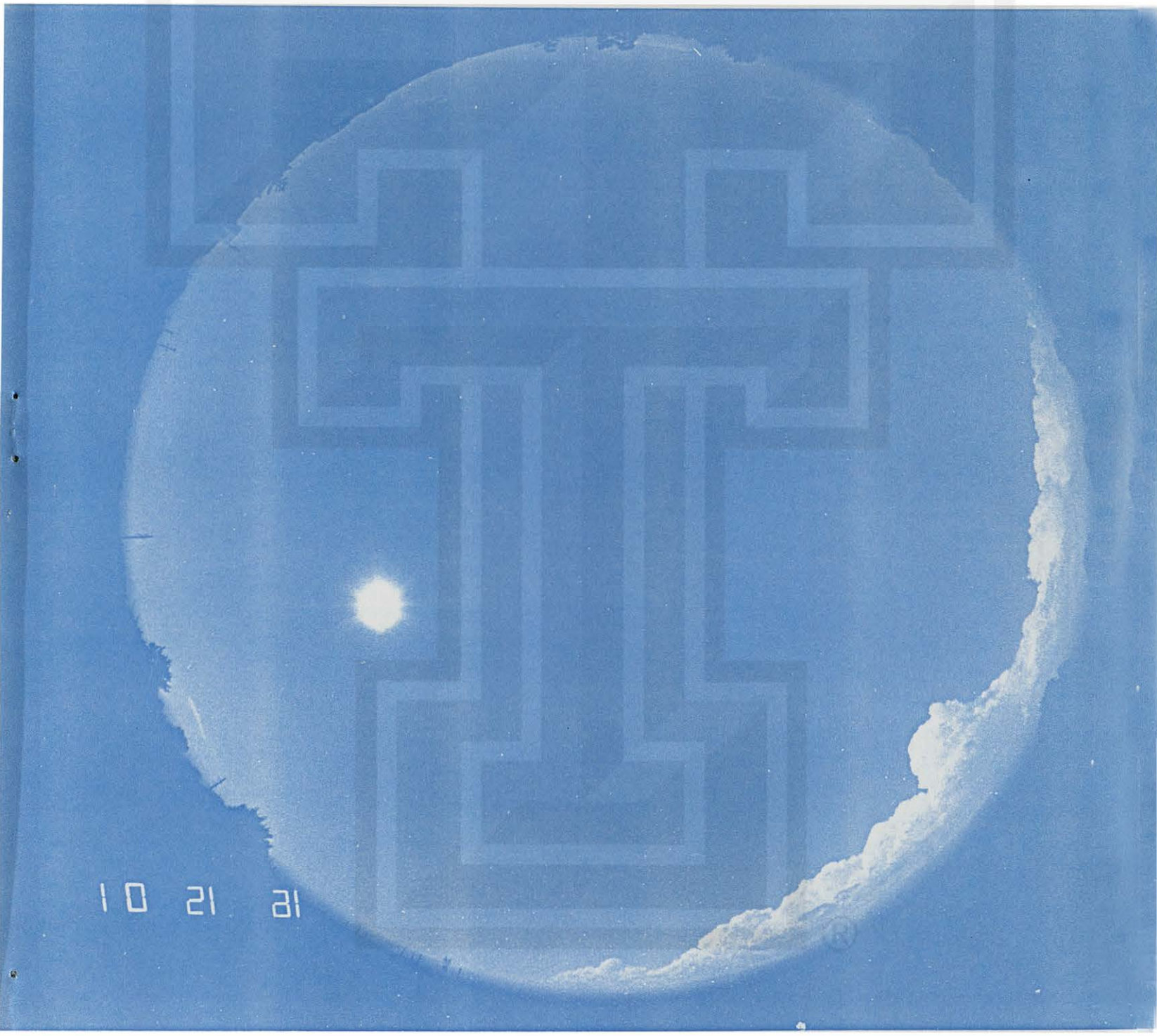

Fig. 5.7

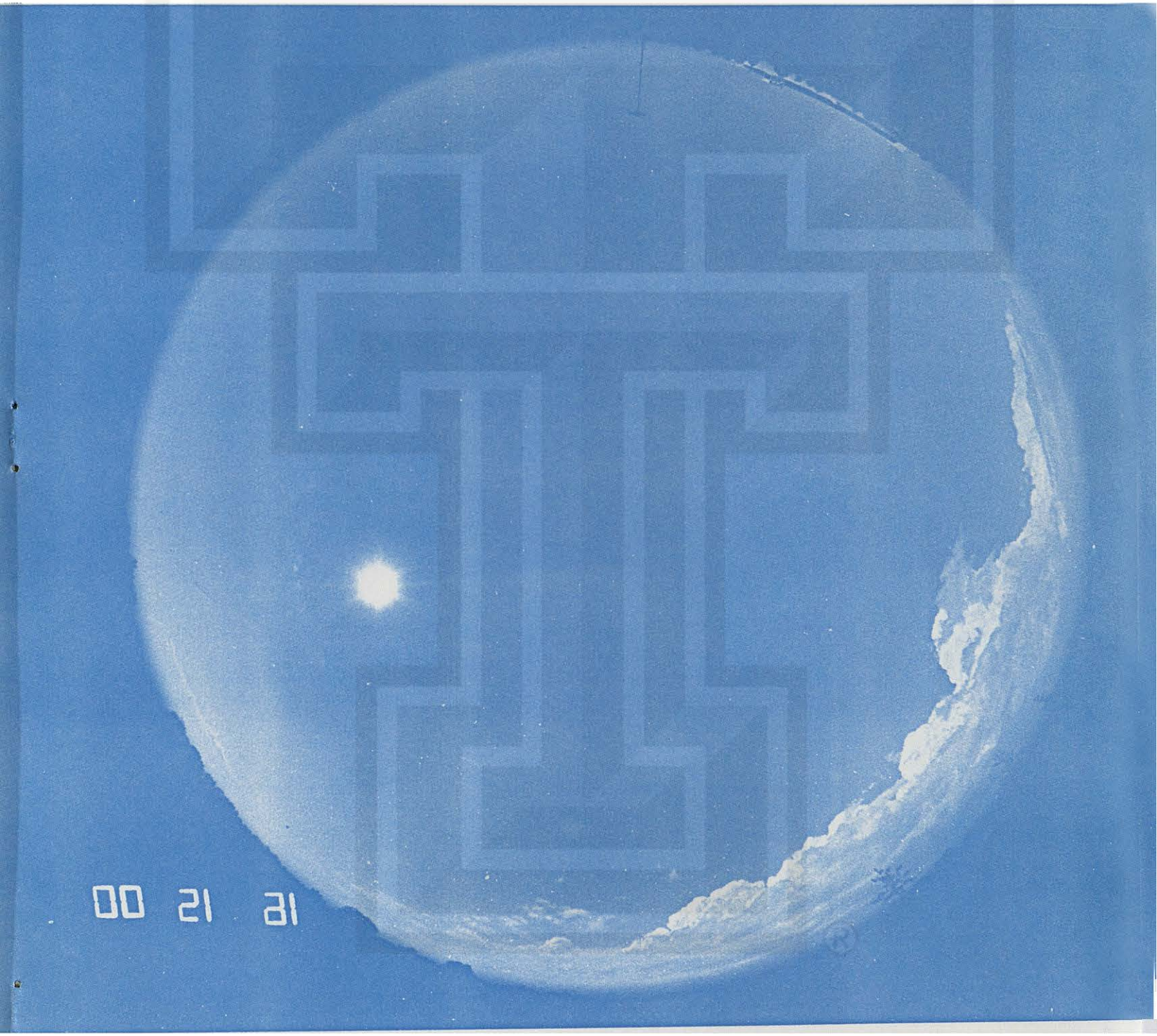

Fig. 5.8

Case 5: Cirrus, Contrails and Alto-cumulus

April 27, 1995 1315-1615 CST Very good high clouds, with multi-level cirrus in all directions from 1315-1515 CST. Besides the cirrus, several contrails could be trackable as well. Between 1515-1615 CST conditions were nearly perfect, with thin cirrus everywhere in addition to alto-cumulus to the west, which was more distinct. These conditions continued until the end of the operation at 1615 CST. This was by far the best day of operation, with rapid-scan data available throughout. Tracking can be done for several types of clouds throughout the period, since there were multi-layer clouds and contrails during the three hours of operation. (Figs. 5.9-5.10)

1531 C 27 Apr 95 North

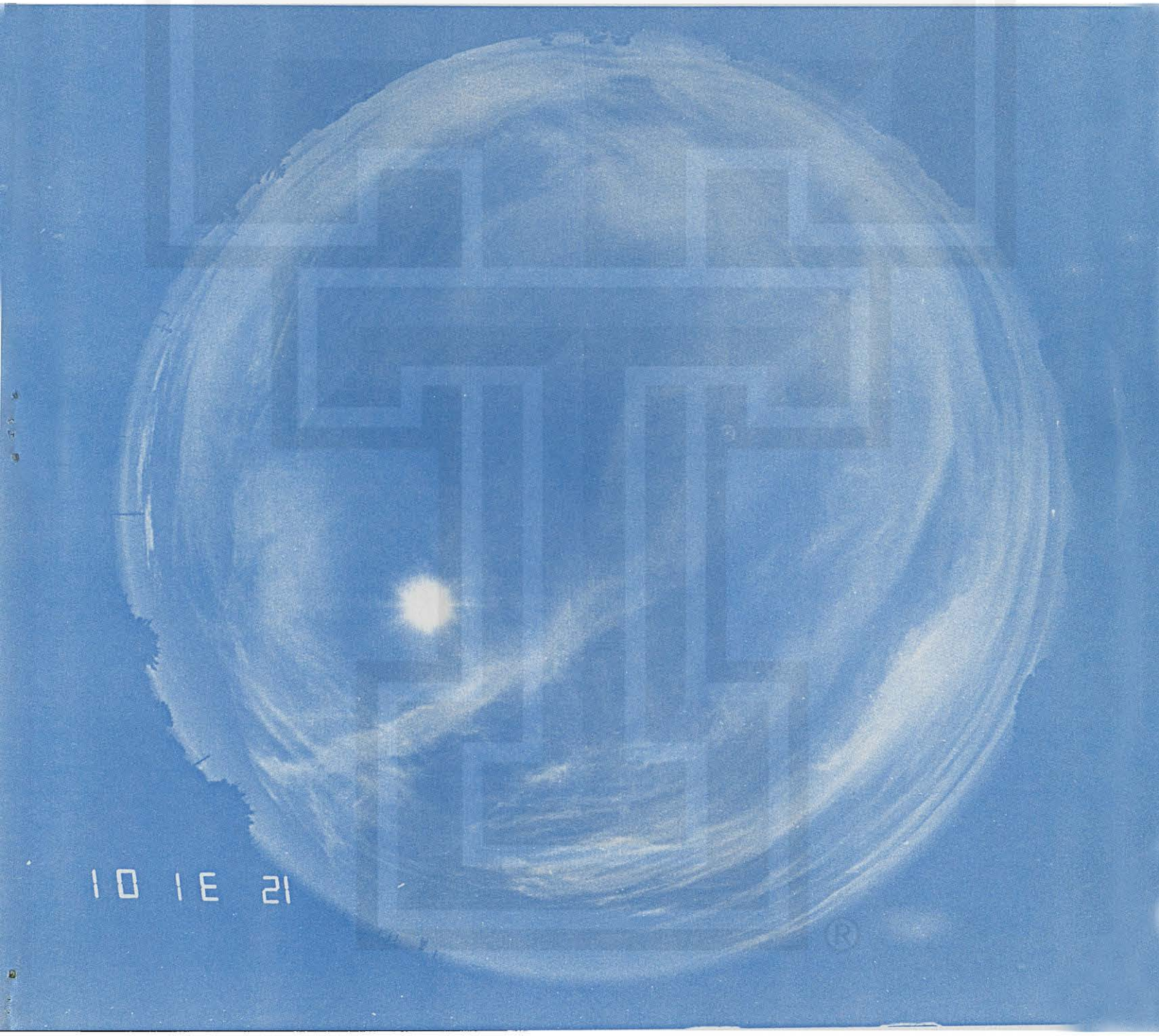

Fig. 5.9

Fig. 5.10

6. SUMMARY AND RECOMMENDATIONS

The knowledge gained in previous cloud motion studies, proved to be invaluable for finding the proper sites for the whole-sky cameras. By locating the cameras on a baseline of 9.59 km. and having a large number of objects along the horizon, a more accurate horizon radius was obtained for each image, compared to previous CHAMEX operations. This accuracy will translate in better results when the tracking of clouds, and the height and motion will be computed.

Because of uncooperative weather during the experiment period, there were only a handful of cases that can be studied for cloud height and motion computations. However, the case of 27 April was a near-perfect day for high and middle cloud conditions, with a complete data set of rapid-scan satellite. This day alone could yield several good time intervals to track clouds and compare the results with satellite. The other potential days of research should still provide good results in the tracking of clouds but the comparison to satellite will be more limited.

The recommendation will be to compare our best photo times with GOES-8 images from the University of Wisconsin, especially during rapid-scan periods. Although only one case, 27 April, had complete rapid-scan pictures during the whole-sky operation, a couple of other cases had some short intervals where cirrus clouds could be tracked (19 and 25 April). For the cases without any rapid-scan, whole-sky stereoscopic cloud height and motions can still be computed, but comparison to satellite will be more difficult. In analyzing whole-sky pictures, one or several smaller periods, ranging 6-12 minutes each, must be chosen from within a case. These whole-sky periods must coincide with the best GOES-8 satellite images. Once these periods of good whole-sky and GOES-8 images are selected to compare, the process of identifying, tracking, and calculating height and motions of clouds can be performed.